Chapter 2
Statistical Aspects of Wave Scattering at Rough Surfaces

A. Sentenac and J. Daillant

2.1 Introduction

The surface state of objects in any scattering experiment is, of necessity, rough. Irregularities are of the most varied nature and length scales, ranging from the atomic scale, where they are caused by the inner structure of the material, to the mesoscopic and macroscopic scale where they can be related to the defects in processing in the case of solid bodies or to fluctuations in the case of liquid surfaces (ocean waves, for example).

The problem of wave scattering at rough surfaces has thus been a subject of study in many research areas, such as medical ultrasonic, radar imaging, optics or solid state physics [1–4]. The main differences stem from the nature of the wavefield and the wavelength of the incident radiation (which determines the scales of roughness that have to be accounted for in the models). When tackling the issue of modelling a scattering experiment, the first difficulty is to describe the geometrical aspect of the surface. In this chapter, we are interested solely in surface states that are not well controlled so that the precise defining equation of the surface, $z = z(x,y)$, is unknown or of little interest. One has (or needs) only information on certain statistical properties of the surface, such as the height repartition or height to height correlations. In this probabilistic approach, the shape of the rough surface is described by a random function of space coordinates (and possibly time as well). The wave scattering problem is then viewed as a statistical problem consisting in finding the statistical characteristics of the scattered field (such as the mean value or field correlation functions), the statistical properties of the surface being given.

In the first section of this contribution we present the statistical techniques used to characterise rough surfaces. The second section is devoted to the description of a surface scattering experiment from a conceptual point of view. In the third section, we investigate to what extent the knowledge of the field statistics such as the mean field or field autocorrelation is relevant for interpreting the data of a scattering experiment which deals necessarily with deterministic rough samples. Finally, we

A. Sentenac (✉)
Institut Fresnel, Campus de Saint Jérôme, av. Escadrille Normandie
13397 Marseille Cedex 20, France

Sentenac, A., Daillant, J.: *Statistical Aspects of Wave Scattering at Rough Surfaces*. Lect. Notes Phys. **770**, 59–84 (2009)
DOI 10.1007/978-3-540-88588-7_2

derive in the fourth section a simple expression of the scattered field and scattered intensity from random rough surfaces under the Born approximation.

2.2 Description of Randomly Rough Surfaces

2.2.1 Introduction

Let us first consider the example of a liquid surface. The exact morphology of the surface is rapidly fluctuating with time and is not accessible inasmuch as the detector will integrate over many different surface shapes. However, statistical information can be obtained and it provides an useful insight on the physical processes. Indeed, these fluctuations obey Boltzmann statistics and are characterised by a small number of relevant parameters such as the density of the liquid or its surface tension (see Sect. 4.5).

We now consider a set of surfaces of artificial origin (such as metallic optical mirrors) that have undergone similar technological treatments (like polishing and cleaning). Since it is impossible to reproduce all the microscopic factors affecting the surface state, these surfaces have complex and completely different defining equations $z = z(x,y)$. However, if the surface processing is well enough controlled, they will present some similarities, of statistical nature, that will distinguish them from surfaces that have received a totally different treatment.

In these two examples, we are faced with the issue of describing a set of real surfaces which present similar statistical properties and whose defining equations $z(x,y)$ are unknown or of small interest (see Fig. 2.1). It appears convenient [2] to approximate this set of surfaces by a statistical ensemble of surfaces that are realisations of a random continuous process of the plane coordinates $\mathbf{r}_{\|} = (x,y)$, whose statistical properties depend on some relevant parameters of the physical processes affecting the surface state (like the grain size of the polishing abrasive in the case of surfaces of artificial origin). It is likely that the characteristic functions $z(\mathbf{r}_{\|})$ of the surfaces generated by the random process will be different from that of the real surfaces under study, but the statistical properties of both ensembles should be the same.

2.2.2 Height Probability Distributions

Generally speaking, a random rough surface is completely described statistically by the assignment of the n-point ($n \to \infty$) height probability distribution $p_n(\mathbf{r}_{1\|}, z_1 \ldots \mathbf{r}_{n\|}, z_n)$ where $p_n(\mathbf{r}_{1\|}, z_1 \ldots \mathbf{r}_{n\|}, z_n) dz_1 \ldots dz_n$ is the probability for the surface points of plane coordinates $\mathbf{r}_{1\|}, \ldots, \mathbf{r}_{n\|}$ of being at the height between $(z_1 \ldots z_n)$ and $(z_1 + dz_1 \cdots z_n + dz_n)$. However, in most cases, we restrict the description of the randomly rough surface to the assignment of the one- and two-point distribution functions

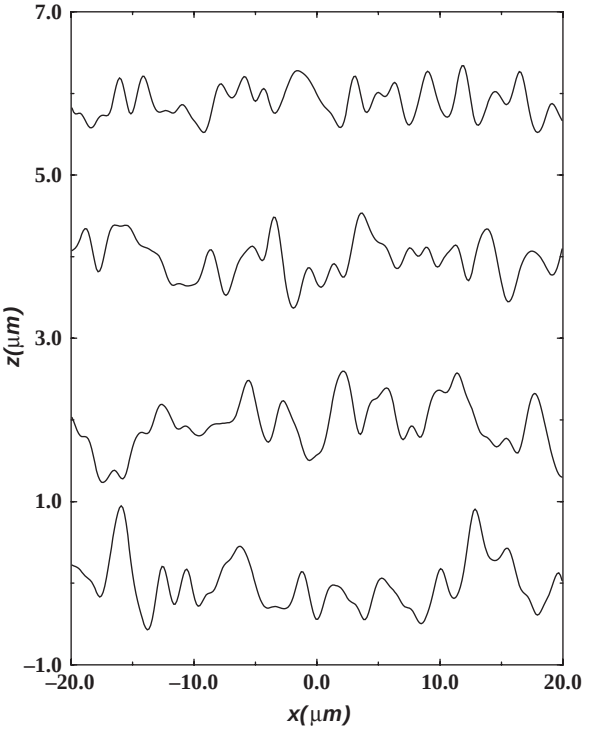

Fig. 2.1 Examples of various rough surfaces that present the same Gaussian statistical properties

$p_1(\mathbf{r}_\parallel, z)$ and $p_2(\mathbf{r}_{1\parallel}, z_1; \mathbf{r}_{2\parallel}, z_2)$. Indeed, most scattering theories need solely this information.

From these probability functions, one can calculate the ensemble average of any functional of the random variables $(z_1 \dots z_n)$ where $z_i = z(\mathbf{r}_{i\parallel \mathbf{r}_{i\parallel}})$, through the integral,

$$\langle F \rangle (\mathbf{r}_{1\parallel} \dots \mathbf{r}_{n\parallel}) = \int_{-\infty}^{\infty} F(z_1 \dots z_n) p_n(\mathbf{r}_{1\parallel}, z_1 \dots \mathbf{r}_{n\parallel}, z_n) dz_1 \dots dz_n. \tag{2.1}$$

The domain of integration covers all the possible values for $(z_1 \dots z_n)$. This quantity is equivalent to an average of F calculated over an ensemble of surface realisations S_p,

$$\langle F \rangle (\mathbf{r}_{1\parallel} \dots \mathbf{r}_{n\parallel}) = \lim_{N \to \infty} \frac{1}{N} \sum_{p=1}^{N} F(z_1^p \dots z_n^p), \tag{2.2}$$

where z_j^p is the altitude of the pth surface realisation at plane coordinates $\mathbf{r}_{j\parallel}$.

With this definition, one obtains in particular the mean height of the surface through

$$\langle z \rangle (\mathbf{r}_\parallel) = \int_{-\infty}^{\infty} z(\mathbf{r}_\parallel) p_1(\mathbf{r}_\parallel, z) dz. \tag{2.3}$$

The mean square height of the surface is given by

$$\langle z^2\rangle(\mathbf{r}_\parallel) = \int_{-\infty}^{\infty} z^2(\mathbf{r}_\parallel)\, p_1(\mathbf{r}_\parallel, z)\, dz. \tag{2.4}$$

The height–height correlation function C_{zz} is defined by

$$C_{zz}(\mathbf{r}_{1\parallel}, \mathbf{r}_{2\parallel}) = \langle z_1 z_2\rangle = \int_{-\infty}^{\infty} z_1 z_2\, p_2(\mathbf{r}_{1\parallel}, z_1, \mathbf{r}_{2\parallel}, z_2)\, dz_1 dz_2, \tag{2.5}$$

where $z_j = z(\mathbf{r}_{j\parallel})$. It is also usual to introduce the pair-correlation function $g(\mathbf{r}_{1\parallel}, \mathbf{r}_{2\parallel})$ which averages the square of the difference in height between two points of the surface,

$$g(\mathbf{r}_{1\parallel}, \mathbf{r}_{2\parallel}) = \langle (z_1 - z_2)^2\rangle = \int_{-\infty}^{\infty} (z_1 - z_2)^2\, p_2(\mathbf{r}_{1\parallel}, z_1, \mathbf{r}_{2\parallel}, z_2)\, dz_1 dz_2. \tag{2.6}$$

Note that $g(\mathbf{r}_{1\parallel}, \mathbf{r}_{2\parallel}) = 2\langle z^2\rangle(\mathbf{r}_\parallel) - 2C_{zz}(\mathbf{r}_{1\parallel}, \mathbf{r}_{2\parallel})$.

2.2.3 Homogeneity and Ergodicity

Randomly rough surfaces have frequently the property that the character of the height fluctuations z does not change with the location on the surface. More precisely, if all the probability distribution functions p_i are invariant under any arbitrary translation of the spatial origin, the random process is called homogeneous. As a consequence, the ensemble average of the functional $F(z_1 \ldots z_n)$ will depend only on the vector difference, $\mathbf{r}_{j\parallel} - \mathbf{r}_{1\parallel}$, between one of the n space argument $\mathbf{r}_{1\parallel}$ and the $(n-1)$ remaining others $\mathbf{r}_{j\parallel},\ j = 2 \ldots n$.

$$\langle F\rangle(\mathbf{r}_{1\parallel}, \ldots, \mathbf{r}_{n\parallel}) = \langle F\rangle(\mathbf{0}_\parallel \ldots \mathbf{r}_{n\parallel} - \mathbf{r}_{1\parallel}). \tag{2.7}$$

When the random process is isotropic (i.e. has the same characteristics along any direction) the dependencies reduce to the distance $|\mathbf{r}_{j\parallel} - \mathbf{r}_{1\parallel}|$ between one of the space argument and the others. Hereafter we will only consider homogeneous isotropic random processes and we propose a simplified notation for the various functions already introduced.

The mean altitude $\langle z\rangle(\mathbf{r}_\parallel)$ does not depend on the $\mathbf{r}_\parallel$ position and one can find a reference plane surface such as $\langle z\rangle = 0$. The mean square deviation of the surface is also a constant and we define the root mean square (rms) height σ as

$$\sigma^2 = \langle z^2\rangle = \int_{-\infty}^{\infty} z^2 p_1(z)\, dz. \tag{2.8}$$

The rms height is often used to give an indication of the "degree of roughness", the larger the σ the rougher the surface. Note that the arguments of the probability distribution are much simpler.

Similarly, the height–height correlation function can be written as

$$C_{zz}(\mathbf{r}_{1\|},\mathbf{r}_{2\|}) = \langle z(\mathbf{0}_\|)z(\mathbf{r}_\|)\rangle = C_{zz}(r_\|) = \int z_1 z_2 p_2(z_1,z_2,r_\|)dz_1 dz_2, \tag{2.9}$$

where $r_\| = |\mathbf{r}_\||$. We also introduce, with these simpler notations, the one-point and two-point characteristic functions,

$$\chi_1(s) = \int_{-\infty}^{\infty} p_1(z)e^{isz}dz, \tag{2.10}$$

$$\chi_2(s,s',r_\|) = \int_{-\infty}^{\infty} p_2(z,z',r_\|)e^{isz+is'z'}dzdz'. \tag{2.11}$$

One of the most important attributes of a homogeneous random process is its power spectrum, $P(\mathbf{q}_\|)$, that gives an indication of the strength of the surface fluctuations associated with a particular wavelength. Roughly speaking, the rough surface is regarded as a superposition of gratings with different periods and heights. The power spectrum is a tool that relates the height to the period. We introduce the Fourier transform of the random variable z,

$$\tilde{z}(\mathbf{q}_\|) = \int z(\mathbf{r}_\|)e^{i\mathbf{q}_\|\cdot\mathbf{r}_\|}d\mathbf{r}_\|, \tag{2.12}$$

where $\mathbf{q}_\| = (q_x, q_y)$ is the in-plane wave-vector transfer. We define the spectrum as

$$P(\mathbf{q}_\|) = \langle|\tilde{z}(\mathbf{q}_\|)|^2\rangle = \langle\tilde{z}(\mathbf{q}_\|)\tilde{z}(-\mathbf{q}_\|)\rangle. \tag{2.13}$$

The Wiener–Khintchine theorem [5] states that the power spectrum is the Fourier transform of the correlation function:

$$P(\mathbf{q}_\|) = \int d\mathbf{r}_\| e^{i\mathbf{q}_\|\cdot\mathbf{r}_\|}\langle z(\mathbf{0}_\|)z(\mathbf{r}_\|)\rangle = 4\pi^2\tilde{C}_{zz}(\mathbf{q}_\|). \tag{2.14}$$

More precisely, one shows that

$$\langle\tilde{z}^*(\mathbf{q}_\|)\tilde{z}(\mathbf{q}'_\|)\rangle = \langle\tilde{z}(-\mathbf{q}_\|)\tilde{z}(\mathbf{q}'_\|)\rangle = 4\pi^2\tilde{C}_{zz}(\mathbf{q}_\|)\delta(\mathbf{q}_\| - \mathbf{q}'_\|). \tag{2.15}$$

The Fourier components of a homogeneous random variable are independent random variables, whose mean square dispersion is given by the Fourier transform of the correlation function. If the power spectrum decreases slowly with increasing $q_\|$, the roughness associated to small periods will remain important. Thus, whatever the length scale, the surface will present irregularities. In the real space, it implies that the correlation between the heights of two points on the surface will be small, whatever their separation. As a result, the correlation function will exhibit a singular behaviour about 0 (discontinuity of the derivative for example). An illustration of the influence of the correlation function (or power spectrum) on the roughness aspect of the surface is presented in Fig. 2.2 and detailed in Sect. 2.2.4 in the special case of a Gaussian distribution of heights.

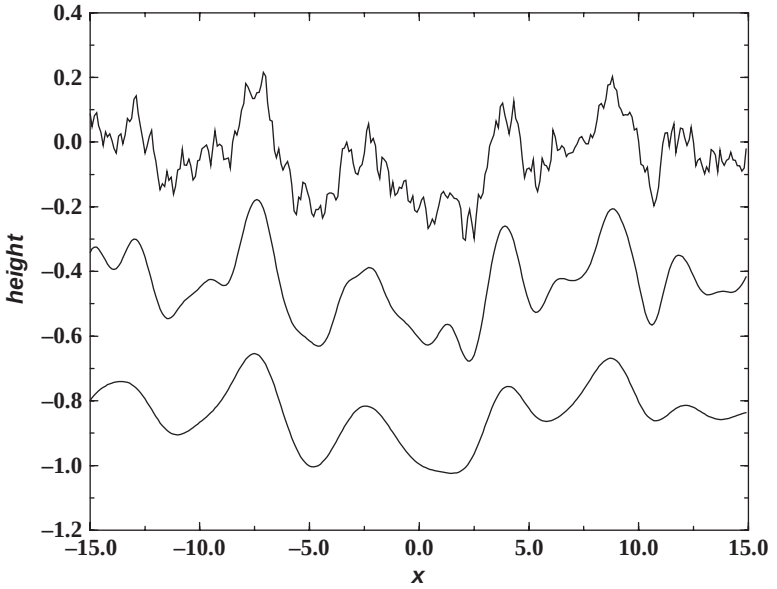

Fig. 2.2 Various rough surfaces with Gaussian height distribution but various correlation functions. From bottom to top, $C_{zz}(R) = \sigma^2\xi^4/(\xi^2+R^2)^2$, $C_{zz}(R) = \sigma^2\exp(-\frac{R^2}{\xi^2})$, $C_{zz}(R) = \sigma^2\exp(-\frac{R}{\xi})$

Until now we have been interested solely in ensemble average, which necessitates the knowledge of the complete set of rough surfaces generated by the homogeneous random process (or the probability distributions). However, sometimes only a single realisation S_p (with dimension L_x, L_y along Ox and Oy) of the random process is available and one defines the spatial average of any functional $F(z_1,\ldots,z_n)$ for this surface by

$$\bar{F_p}(\mathbf{0}_\parallel,\ldots,\mathbf{r}_{n\parallel}) = \lim_{L_x\times L_y\to\infty}\frac{1}{L_xL_y}\int_{L_x\times L_y} d\mathbf{r}'_\parallel F[z(\mathbf{r}'_\parallel)\ldots z(\mathbf{r}'_\parallel+\mathbf{r}_{n\parallel})]. \tag{2.16}$$

It happens frequently that each realisation of the ensemble carries the same statistical information about the homogeneous random process as every other realisation. The spatial averages calculated for any realisation are then all equal and coincide with the ensemble average. The homogeneous random process is then said to be an ergodic process. In this case, the following particular relations hold:

$$\sigma^2 = \langle z^2\rangle = \lim_{L_x,L_y\to\infty}\frac{1}{L_xL_y}\int_{L_x\times L_y} z^2(\mathbf{r}_\parallel)d\mathbf{r}_\parallel, \tag{2.17}$$

$$C_{zz}(r_\parallel) = \langle z(\mathbf{0}_\parallel)z(\mathbf{r}_\parallel)\rangle = \lim_{L_x,L_y\to\infty}\frac{1}{L_xL_y}\int_{L_x\times L_y} z(\mathbf{r}'_\parallel)z(\mathbf{r}'_\parallel+\mathbf{r}_\parallel)d\mathbf{r}'_\parallel. \tag{2.18}$$

One can show that Eqs. (2.17) and (2.18) will be satisfied if the correlation function $C_{zz}(r_\parallel)$ dies out sufficiently rapidly with increasing $r_\parallel$ (see for demonstration [5]).

Indeed, this property implies that one realisation of the rough surface can be divided up into subsurfaces of smaller area that are uncorrelated so that an ensemble of surfaces can be constructed from a single realisation. Spatial averaging amounts then to ensemble averaging. If the random process is homogeneous and ergodic, all the realisations will look similar while differing in detail. This is exactly what we expect in order to describe liquid surfaces varying with time or set of surfaces of artificial origin. The fact that spatial averaging is equivalent to ensemble averaging when the surface contains enough correlation lengths to recover all the information about the random process is of crucial importance in statistical wave scattering theory.

2.2.4 The Gaussian Probability Distribution and Various Correlation Functions

In most theories, the height probability distribution is taken to be Gaussian. The Gaussian distribution plays a central role because it has an especially simple structure and, because of the central limit theorem, it is a probability distribution that is encountered under a great variety of different conditions. If the height z of a surface is due to a large number of local independent events whose effects are cumulative (like the passage of grain abrasive), the resulting altitude will obey nearly Gaussian statistics. This result is a manifestation of the central limit theorem which states that if a random variable X is the sum of N independent random variables x_i, it will have a Gaussian probability distribution in the limit of large N. Hereafter, we suppose that the average value of the Gaussian variate $z(\mathbf{r}_\parallel)$ is null, $\langle z\rangle = 0$. The Gaussian height distribution function is written as

$$p_1(z) = \frac{1}{\sigma\sqrt{2\pi}} \exp\left(-\frac{z^2}{2\sigma^2}\right). \tag{2.19}$$

Gaussian variates have the remarkable property that the random process is entirely determined by the height probability distribution and the height–height correlation function C_{zz}. All higher order correlations are expressible in terms of second-order correlation [5]. The two-point distribution function is given in this case by

$$p_2(z,z',r_\parallel) = \frac{1}{2\pi\sqrt{\sigma^4 - C_{zz}^2(r_\parallel)}} \exp - \left[\frac{\sigma^2(z^2+z'^2) - 2zz'C_{zz}(r_\parallel)}{2\sigma^4 - 2C_{zz}^2(r_\parallel)}\right]. \tag{2.20}$$

Other useful results on the Gaussian variates are

$$\chi_1(s) = \langle e^{isz}\rangle = e^{-s^2\sigma^2/2}, \tag{2.21}$$

$$\chi_2(s,s',r_\parallel) = \left\langle e^{i(sz-s'z')}\right\rangle = e^{-\sigma^2(s^2+s'^2)/2} e^{ss'C_{zz}(r_\parallel)}. \tag{2.22}$$

The correlation function plays a fundamental role in the surface aspect. It provides an indication of the length scales over which height changes along the surface. It gives in particular the distance beyond which two points of the surface can be considered independent. If the surface is truly random, $C_{zz}(r_{\|})$ decays to zero with increasing $r_{\|}$. The simplest and often used form for the correlation function is also Gaussian,

$$C_{zz}(r_{\|}) = \sigma^2 \exp(-r_{\|}^2/\xi^2). \tag{2.23}$$

The correlation length ξ is the typical distance between two different irregularities (or bumps) on the surface. Beyond this distance, the heights are not correlated.

In certain scattering experiments, one can retrieve the behaviour of the correlation function for $r_{\|}$ close to zero. We have thus access to the small scale properties of the surface. We have seen that the regularity of the correlation function at zero mirrors the asymptotic behaviour of the power spectrum: the faster the high-frequency components of the surface decay to zero, the smoother the correlation function about zero. The Gaussian scheme whose variations about zero have the quadratic form $\sigma^2(1-(r_{\|}/\xi)^2)$ is thus indicated solely for surfaces that present only one typical lateral length scale [6].

For surfaces with structures down to arbitrary small scales, one expects the correlation function to be more singular at zero. An example is the self-affine rough surface for which

$$g(r_{\|}) = A_0 r_{\|}^{2h}, \tag{2.24}$$

where A_0 is a constant, or

$$C_{zz}(r_{\|}) = \sigma^2 \left(1 - \frac{r_{\|}^{2h}}{\xi^{2h}}\right), \tag{2.25}$$

with $0 < h < 1$. The roughness exponent or Hurst exponent h is the key parameter which describes the height fluctuations at the surface: small h values produce very rough surfaces while if h is close to 1 the surface is more regular. This exponent is associated to fractal surfaces with dimension $D = 3-h$ as reported by Mandelbrodt [7]. The pair-correlation function given in Eq. (2.24) diverges for $r_{\|} \to \infty$. Hence, all the length scales along the vertical axis are represented and the roughness of the surface cannot be defined. We will see below that in that case, there is no specular reflection. However, very often, some physical processes limit the divergence of the correlation function, i.e. the roughness saturates at some in-plane cut-off ξ. Such surfaces are well described by the following correlation function,

$$C_{zz}(R) = \sigma^2 \exp\left(-\frac{R^{2h}}{\xi^{2h}}\right). \tag{2.26}$$

For liquid surfaces other functional forms described in Sect. 4.5 are used.

2.2.5 More Complicated Geometries: Multilayers and Volume Inhomogeneities

Up to now we have considered solely the statistical description of a rough surface separating two homogeneous media. The mathematical notions that have been introduced can be generalised to more complicated problems such as stacks of rough surfaces in multilayer components. In this case, one must also consider the correlation function between the different interfaces, $\langle z_i(\mathbf{0}_\parallel) z_j(\mathbf{r}_\parallel)\rangle$, where z_i represents the height of the i th surface. A detailed description of the statistics of a rough multilayer is given in Sect. 6.2. One can also describe in a similar fashion the random fluctuations of the refractive index (or electronic density) ρ. In this case ρ is a random continuous variable of the three-dimensional space coordinates $(\mathbf{r}_\parallel, z)$. It will be introduced in Sects. 4.3.3 and 7.3.

2.3 Description of a Surface Scattering Experiment, Coherence Domains

We have seen how to characterise, with statistical tools, the rough surface geometry. The next issue is to relate these statistics to the intensity scattered by the sample in a scattering experiment. In this section, we introduce the main theoretical results that describe the interaction between electromagnetic waves and surfaces. Attention is drawn on the notion of "coherence domains" which takes on particular importance in the modelling of scattering from random media. In this foreword, we present briefly the basic mechanisms that subtend this concept.

It can be shown (bear in mind the Huygens–Fresnel principle or see Sect. 4.1.4) that a rough surface illuminated by an electromagnetic incident field acts as a collection of radiating secondary point sources. The superposition of the radiation of those sources yields the total diffracted field. If the secondary sources are coherently illuminated, the total diffracted field is the sum of the complex amplitudes of each secondary diffracted beam. In other words, one has to account for the phase difference in this superposition. As a result, an interference pattern is created. The coherence domain is the surface region in which all the radiating secondary sources interfere. It depends trivially on the nature of the illuminating beam (which can be partially coherent), but more importantly, it depends on the angular resolution of the detector. To illustrate this assertion, we consider the Young's holes experiment [8]. Light from a monochromatic point source (or a coherent beam) falls on two pinholes located in the sample plane (see Fig. 2.3). We study the transmitted radiation pattern on a screen parallel to the sample plane at a distance D. In this region, an interference pattern is formed. The periodicity Λ of the fringes, which is the signature of the coherence between the two secondary sources, depends on the separation d between the two pinholes, $\Lambda = \lambda D/d$. Suppose now that a detector is moved on the screen to record the diffracted intensity. As long as the detector width l is close

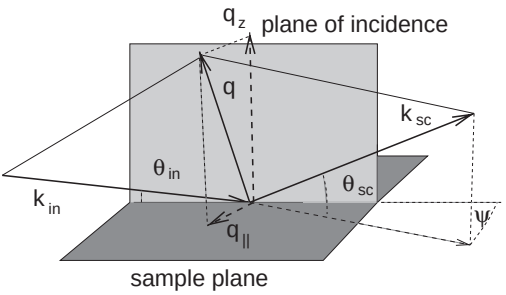

Fig. 2.3 Scattering geometry for interpreting surface scattering

to Λ, the modulation of the interference pattern will be detected. On the contrary, if $l > 10\Lambda$ the intensity measured by the detector is the average of the fringe intensities. We obtain a constant equal to the sum of the intensities scattered by each secondary source. In this case, one may consider that from the detector point of view, the sources radiate in an incoherent way. We see with this simple experiment that the coherence length is directly linked to the finite extent of the detector (equivalent to a finite angular resolution).[1]

We now turn to a more accurate description of a surface scattering experiment.

2.3.1 Scattering Geometry

We consider an ideal scattering experiment consisting in illuminating a rough sample with a (perfectly coherent monochromatic) beam directed along $\mathbf{k}_{\text{in}}$ and detecting the flux of Poynting vector in an arbitrary small solid angle in the direction $\mathbf{k}_{\text{sc}}$ with a point-like detector located in the far-field region.

The interaction of the beam with the material results in a wave-vector transfer,

$$\mathbf{q} = \mathbf{k}_{\text{sc}} - \mathbf{k}_{\text{in}}. \tag{2.27}$$

Figure 2.3 shows the scattering geometry in the general case of a surface experiment. The plane of incidence contains the incident wave vector $\mathbf{k}_{\text{in}}$ and the normal to the surface Oz. In a reflectivity experiment, it is usual to work in the plane of incidence and thus to have $\psi = 0$. Yet the case $\psi \neq 0$ is of special interest for surface diffraction experiments in grazing incidence geometry. When working in the plane of incidence it is also useful to distinguish the symmetric specular geometry for which $\theta_{\text{in}} = \theta_{\text{sc}}$ and the off-specular geometry for which $\theta_{\text{in}} \neq \theta_{\text{sc}}$. The following set of Eq. (2.28) gives the components of the wave-vector transfer with the notations introduced in Fig. 2.3:

[1] It is also obviously linked to the degree of coherence fixed by, for example, the incidence slit opening. However, for x-ray or neutron experiments the resolution is actually generally limited by the detector slits opening.

$$\begin{cases} q_x = k_0\,(\cos\theta_{\rm sc}\cos\psi - \cos\theta_{\rm in}) \\ q_y = k_0\,(\cos\theta_{\rm sc}\sin\psi) \\ q_z = k_0\,(\sin\theta_{\rm sc} + \sin\theta_{\rm in}) \end{cases} . \tag{2.28}$$

2.3.2 Scattering Cross-Section

In the ideal experimental setup presented in the previous section, one exactly measures the differential scattering cross-section as described in Fig. 1.1 (the isolated scattering object is the rough sample in this case). The vectorial electric field $\mathbf{E}$ is written as the sum,

$$\mathbf{E} = \mathbf{E}_{\rm in} + \mathbf{E}_{\rm sc}, \tag{2.29}$$

of the incident plus scattered field. We are interested by the flux of the Poynting vector $\mathbf{S}$ through a surface dS located at the position $\mathbf{R}$ of the detector for a unit incident flux. The precise calculations of the differential scattering cross-section are detailed in Sect. 4.1.4. In this paragraph, we simply introduce the main steps of the derivation.

One assumes that the detector located at $\mathbf{R}$ is placed far from the sample (far-field approximation). We define the scattering direction by the vector $\mathbf{k}_{\rm sc}$ (see Fig. 2.3),

$$\mathbf{k}_{\rm sc} = k_0\widehat{\mathbf{u}} = k_0\mathbf{R}/R. \tag{2.30}$$

It is shown in Sect. 4.1.4 that the scattered field can be viewed as the sum of the wavelets radiated by the electric dipoles induced in the material by the incident field (these radiating electric dipoles are the coherent secondary sources presented in the introduction). The strength of the induced dipole located at $\mathbf{r}'$ in the sample is given by the total field times the permittivity contrast at this point, $[k^2(\mathbf{r}') - k_0^2]\mathbf{E}(\mathbf{r}')$. Let us recall that for x-rays,

$$(k^2(\mathbf{r}') - k_0^2) = k_0^2[n^2(\mathbf{r}') - 1] = -4\pi r_e \rho_{el}(\mathbf{r}'), \tag{2.31}$$

where ρ_{el} is the local electron density and r_e the classical electron radius.[2] In the far-field region, the scattered field can be written as, see Eq. (4.19) (the far-field approximation and its validity domain are discussed in more detail in Chap. 4),

[2] If one is only interested in materials with low atomic numbers for which the x-ray frequency is much larger than all atomic frequencies, the electrons can be considered as free electrons plunged into an electric field $\mathbf{E}$. In this case, the movement of the electron is governed by $m_e d\mathbf{v}/dt = -e\mathbf{E}$, where m_e, $\mathbf{v}$, $-e$, are the mass, the velocity and the charge of the electron, respectively. We find $\mathbf{v} = (ie/m_e\omega)\mathbf{E}$ for a $e^{i\omega t}$ time dependence of the electric field. Thus, the current density is $\mathbf{j} = -e\rho_{el}\mathbf{v} = -(ie^2\rho_{el}/m_e\omega)\mathbf{E}$ where ρ_{el} is the local electron density. Writing the Maxwell's equations in the form $curl\mathbf{H} = \mathbf{j} + \epsilon_0\partial\mathbf{E}/\partial t = \partial\mathbf{D}/\partial t = n^2\epsilon_0\partial\mathbf{E}/\partial t$ (depending on whether the system is viewed as a set of electrons in a vacuum or as a material of refractive index n), one obtains by identification that $n = 1 - (e^2/2m_e\epsilon_0\omega^2)\rho_{el} = 1 - (\lambda^2/2\pi)r_e\rho_{el} \approx 1 - 10^{-6}$, with $r_e = (e^2/4\pi\epsilon_0 m_e c^2)$ the "classical electron radius". A complete and rigorous demonstration is given in [9].

$$\mathbf{E}_{\rm sc}(\mathbf{R}) = \frac{\exp(-ik_0R)}{4\pi R}\int d\mathbf{r}'(k^2(\mathbf{r}') - k_0^2)\mathbf{E}_\perp(\mathbf{r}')e^{i\mathbf{k}_{\rm sc}.\mathbf{r}'}, \tag{2.32}$$

where

$$\mathbf{E}_\perp(\mathbf{r}') = \mathbf{E}(\mathbf{r}') - \widehat{\mathbf{u}}.\mathbf{E}(\mathbf{r}')\widehat{\mathbf{u}} \tag{2.33}$$

represents the component of the electric field that is orthogonal to the direction of propagation given by $\widehat{\mathbf{u}}$. Expression (2.32) shows that the scattered electric field $\mathbf{E}_{\rm sc}(\mathbf{R})$ can be approximated by a plane wave [8] with wave vector $\mathbf{k}_{\rm sc} = k_0\mathbf{R}/R = k_0\widehat{\mathbf{u}}$ and amplitude,

$$\mathbf{E}_{\rm sc}(\mathbf{k}_{\rm sc}) = \mathbf{E}_{\rm sc}(\mathbf{R}). \tag{2.34}$$

The Poynting vector is then readily obtained,

$$\mathbf{S} = \frac{1}{2\mu_0 c}|\mathbf{E}_{\rm sc}(\mathbf{R})|^2\widehat{\mathbf{u}}. \tag{2.35}$$

The flux of the Poynting vector for a unit incident flux (or normalised by the incident flux through a unit surface normal to the propagation direction) yields the differential scattering cross-section in the direction given by $\mathbf{k}_{\rm sc}$,

$$\frac{d\sigma}{d\Omega} = \frac{1}{16\pi^2|\mathbf{E}_{\rm in}|^2}\left|\int [k^2(\mathbf{r}') - k_0^2]\mathbf{E}_\perp(\mathbf{r}')e^{i\mathbf{k}_{\rm sc}.\mathbf{r}'}d\mathbf{r}'\right|^2. \tag{2.36}$$

Note that $d\sigma/d\Omega$ involves a double integration, which can be cast in the form,

$$\frac{d\sigma}{d\Omega} = \frac{1}{16\pi^2|\mathbf{E}_{\rm in}|^2}\int d\mathbf{r}\int d\mathbf{r}'(k^2(\mathbf{r}) - k_0^2)(k^2(\mathbf{r}+\mathbf{r}') - k_0^2)$$
$$\mathbf{E}_\perp(\mathbf{r}).\mathbf{E}_\perp^*(\mathbf{r}+\mathbf{r}')e^{i\mathbf{k}_{\rm sc}.\mathbf{r}'}, \tag{2.37}$$

where u^* stands for the conjugate of u. By integrating formally Eq. (2.32) over the vertical axis, one obtains a surface integral,

$$\mathbf{E}_{\rm sc}(\mathbf{R}) = \frac{\exp(-ik_0R)}{4\pi R}\int \mathscr{E}_\perp(\mathbf{r}'_\parallel, k_{\rm scz})e^{i\mathbf{k}_{\rm sc\parallel}.\mathbf{r}'_\parallel}d\mathbf{r}'_\parallel, \tag{2.38}$$

with

$$\mathscr{E}_\perp(\mathbf{r}'_\parallel, k_{\rm scz}) = \int [k^2(\mathbf{r}') - k_0^2]e^{ik_{\rm scz}z'}\mathbf{E}_\perp(\mathbf{r}')dz'. \tag{2.39}$$

We see that Eq. (2.39) is a one-dimensional Fourier transform, thus the variations of $\mathscr{E}_\perp$ with $k_{\rm scz}$ are directly linked to the thickness of the sample. On the other hand, the variations of $\mathbf{E}_{\rm sc}$ with $\mathbf{k}_{\rm sc\parallel}$ are related to the width of the illuminated area (i.e. the region for which $[k^2(\mathbf{r}') - k_0^2]\mathbf{E}$ is non-zero).

2.3.3 Coherence Domains

Up to now, we have considered an ideal experiment with a point-like detector. In reality, the detector has a finite size and one must integrate the differential scattering

cross-section over the detector solid angle, $\Delta\Omega_{\rm det}$. Since the cross-section is defined as a function of wave vectors, it is more convenient to transform the integration over the solid angle $\Delta\Omega_{\rm det}$ centred about the direction $\mathbf{k}_{sc}$ into an integration in the (k_x, k_y) plane. The measured intensity (scattering cross-section convoluted with the resolution function) is then given by

$$I = \frac{1}{16\pi^2}\frac{1}{|\mathbf{E}_{\rm in}|}\int d\mathbf{k}_{\parallel}\mathscr{R}(\mathbf{k}_{\parallel}) \times \int d\mathbf{r}_{\parallel}\int d\mathbf{r'}_{\parallel}\mathscr{E}_{\perp}^{*}(\mathbf{r}_{\parallel}+\mathbf{r'}_{\parallel},k_z).\mathscr{E}_{\perp}(\mathbf{r}_{\parallel},k_z)e^{i\mathbf{k}_{\parallel}.\mathbf{r'}_{\parallel}}, \tag{2.40}$$

where $\mathscr{R}(\mathbf{k}_{\parallel})$ is the detector acceptance in the (k_x, k_y) plane. The expression of $\mathscr{R}$ in the wave-vector space is not easily obtained. In an x-ray experiment, it depends on the parameters (height, width) of the collecting slits. The reader is referred to Sect. 4.4 for a detailed expression of $\mathscr{R}$ as a function of the detector shape. In this introductory chapter it is sufficient to take for $\mathscr{R}$ a Gaussian function centred about $\mathbf{k}_{\rm sc\parallel}$,

$$\mathscr{R}(k_{\rm scx}, k_{\rm scy}) = C\exp\left[-\frac{(k_x-k_{\rm scx})^2}{2\Delta k_x^2}-\frac{(k_y-k_{\rm scy})^2}{2\Delta k_y^2}\right]. \tag{2.41}$$

The variables $\Delta k_x, \Delta k_y$ govern the angular aperture of the detector. If one assumes that the integrand does not vary significantly along $\mathbf{k}_z$ inside $\Delta k_x\,\Delta k_y$,[3] the resulting intensity is given by

$$I = \frac{1}{16\pi^2}\frac{1}{|\mathbf{E}_{\rm in}|}\int\int d\mathbf{r}_{\parallel}d\mathbf{r'}_{\parallel}\mathscr{E}_{\perp}^{*}(\mathbf{r}_{\parallel}+\mathbf{r'}_{\parallel},k_{\rm scz}).\mathscr{E}_{\perp}(\mathbf{r}_{\parallel},k_{\rm scz})e^{i\mathbf{k}_{\rm sc\parallel}.\mathbf{r'}_{\parallel}}\tilde{\mathscr{R}}(\mathbf{r'}_{\parallel}), \tag{2.42}$$

where

$$\tilde{\mathscr{R}}(\mathbf{r}_{\parallel}) = 2\pi C\Delta k_x\Delta k_y e^{-\frac{1}{2}\Delta k_x^2x^2-\frac{1}{2}\Delta k_y^2y^2}. \tag{2.43}$$

We now examine Eq. (2.38) that gives the scattered field as the sum of the fields radiated by all the induced dipoles in the sample. We see that the electric field radiated in the direction $\mathbf{k}_{\rm sc}$ by the "effective" dipole placed at point $\mathbf{r}_{\parallel}$ is added coherently to the field radiated by another dipole placed at $\mathbf{r}_{\parallel}+\mathbf{r}'_{\parallel}$ whatever the distance between the points. The intensity, measured by an ideal experiment (coherent source and point-like detector), is given by a double integration of infinite extent which contains the incoherent term $|\mathscr{E}_{\perp}(\mathbf{r}_{\parallel},k_{\rm scz})|^2$ and the cross-product (namely the interference term) $\mathscr{E}_{\perp}(\mathbf{r}_{\parallel},k_{\rm scz}).\mathscr{E}_{\perp}^{*}(\mathbf{r}_{\parallel}+\mathbf{r'}_{\parallel},k_{\rm scz})$. When the detector has a finite size, the double integration is modified by the introduction of the resolution function $\tilde{\mathscr{R}}$

[3] This assumption is not straightforward. It is seen in Eq. (2.39) that the thicker the sample, the faster the variations of $\mathscr{E}_{\perp}$ with k_z. In an x-ray experiment, the sample under study is generally a thin film (a couple of microns) and we are interested by the structure along z of the material (multilayers). Hence, the size of the detector is chosen so that its angular resolution permits to resolve the interference pattern caused by the stack of layers. This amounts to saying that the k_z modulation of $\mathscr{E}_{\perp}^{*}(\mathbf{r}_{\parallel}+\mathbf{r'}_{\parallel},k_z).\mathscr{E}_{\perp}(\mathbf{r}_{\parallel},k_z)$ is not averaged in the detector.

which is the Fourier transform of the angular characteristic function of the detector. In our example, $\tilde{\mathscr{R}}$ is a Gaussian whose support in the (x,y) plane is roughly $1/[\Delta k_x \times \Delta k_y]$. This function limits the domain over which the contribution of the cross term to the total intensity is significant. This domain can be called the coherence domain S_{coh} due to the detector. The fields radiated by two points that belong to this domain will add coherently in the detector (the cross term value is important), while the fields coming from two points outside this domain will add incoherently (the cross term contribution is damped to zero). The resulting intensity can be seen as the incoherent sum of intensities that are scattered from various regions of the sample whose sizes coincide with the coherent domain given by the detector. This can be readily understood by rewriting Eq. (2.42) in the form [10],

$$I \propto \sum_{i=1,N} \int_{S_{\mathrm{coh}}} d\mathbf{r}_{\parallel} \int_{S_{coh}} d\mathbf{r}'_{\parallel} \mathscr{E}^{*}_{\perp}(\mathbf{r_i}_{\parallel} + \mathbf{r}_{\parallel} + \mathbf{r}'_{\parallel}, k_{\mathrm{scz}}).\mathscr{E}_{\perp}(\mathbf{r_i}_{\parallel} + \mathbf{r}_{\parallel}, k_{\mathrm{scz}}) e^{i\mathbf{k}_{\mathrm{sc}\parallel}\cdot\mathbf{r}'_{\parallel}} \tilde{\mathscr{R}}(\mathbf{r}'_{\parallel}), \tag{2.44}$$

where $\mathbf{r}_i$ is the centre of the different coherent regions S_{coh}. Hence, integrating the intensity over a certain solid angle is equivalent to summing the intensities (i.e. incoherent process) from various regions of the illuminated sample. This is the main result of this paragraph. *The finite angular resolution of the detector introduces coherence lengths beyond which two radiating sources can be considered incoherent (even though the incident beam is perfectly coherent)*. Note that the plural is not fortuitous, indeed, the angular resolution of the detector can be different in the *xOy* and *xOz* plane, thus the coherent lengths vary along *Ox*, *Oz* and *Oy*. In a typical x-ray experiment (see Sect. 4.4), the sample is illuminated coherently over 5 mm^2 but the angular resolution of the detector yields coherence domains of solely a couple of square microns. More precisely, a detection slit with height 100 µm, width 1 cm placed at 1 m of the sample with $\theta_{\mathrm{sc}} = 10$ mrad limits the coherent length along *Oz* to 1 µm, along *Ox* to 100 µm and that along *Oy* to 10 nm. Finally, in this introductory section, we have restricted our analysis solely to a detector of finite extent. In general, the incident source has also a finite angular resolution. However, coherence domains induced by the incident angular resolution is usually much bigger than that given by the detector angular resolution so that we do not consider it here. (The calculation scheme would be very similar.) A more complete description of the resolution function of the experiment is given in Sect. 4.4.2.

2.4 Statistical Formulation of the Diffraction Problem

In this section, we point out, through various numerical simulations, the pertinence of a statistical description of the surface and of the scattered power for modelling a scattering experiment in which *the rough sample is necessarily deterministic*. The main steps of our analysis are as follows: Within the coherence domain, the field

radiated by the induced dipoles (or secondary sources) of the sample interfere. We call ***speckle*** the complicated intensity pattern stemming from these interferences. The angular resolution of the detector yields an incoherent averaging of the speckle structures (the intensities are added over a certain angular domain). This angular integration can be performed with an ensemble average by invoking

1. The ergodicity property of the rough surface (i.e. we assume that the sample is one particular realisation of an ergodic random process)
2. The equivalence between finite angular resolution and limited coherence domains

It appears finally that the diffused intensity measured by the detector is adequately modelled by the mean square of the electric field viewed as a function of the random variable z. Throughout this section, the numerical examples are given in the optical domain. The wavelength is about $1\,\mu$m and the perfectly coherent incident beam is directed along the Oz axis.

2.4.1 To What Extent Is a Statistical Formulation of the Diffraction Problem Relevant?

In Sect. 2.3 it has been shown how to calculate formally the electromagnetic power measured by the detector in a scattering experiment. To obtain the differential scattering cross-section, one needs to know the permittivity contrast at each point of the sample and the electric field at those points, Eq. (2.37). If the geometry of the sample is perfectly well known (i.e. deterministic like gratings), various techniques (such as the integral boundary method [11,12]) permit to obtain without any approximation the field inside the sample. It is thus possible to simulate with accuracy the experimental results. In the case of scattering by gratings (i.e. periodic surfaces) the good agreement between experimental results and calculations confirms the validity of the numerical simulations [12].

We study the scattered intensity from different rough deterministic surfaces s_n (e.g. those presented in Fig. 2.1) illuminated by a perfectly coherent beam. In this experiment, we suppose that the size of the coherence domains induced by the finite resolution of the detector is close to that of the illuminated area A. In other words, all the fringes of the interference pattern stemming from the coherent sum of the fields radiated by every illuminated point of the surface are resolved by the detector. We observe in Fig. 2.4 that the angular distribution of the intensity scattered by each surface presents a chaotic behaviour. This phenomenon can be explained by recalling that the scattered field consists of many coherent wavelets, each arising from a different microscopic element of the rough surface, see Eq. (2.38). The random height position of these elements yields a random dephasing of the various coherent wavelets which results in a granular intensity pattern. This seemingly random angular intensity behaviour, known as speckle effect, is obtained when the coherence domains include many correlation lengths of the surface, when the roughness is not negligible as compared to the wavelength (so that the random dephasing

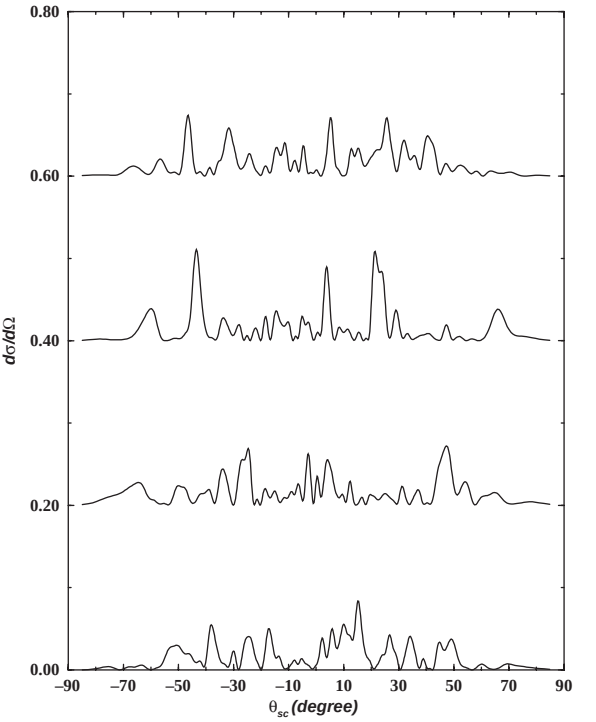

Fig. 2.4 Simulations of the differential scattering cross-section for the surfaces presented in Fig. 2.1. The illuminated area covers 40 μm which explains the large angular width of the speckle. The incident wavelength is 1 μm, the refractive index is $n = 1.5$. Normal incidence. The calculations are performed with a rigorous integral boundary method (no approximation in solving Eq. (2.37) other than the numerical discretisations) [13]

amplitude is important) and most importantly *when the size of the coherence domains is close to that of the illuminated area* so that the speckle is not averaged in the detector. To retrieve the precise angular behaviour of the intensity, one needs an accurate deterministic description of the surface [14]. In Fig. 2.4 the surfaces s_n present totally different intensity patterns even though they have the same statistical properties. However, some similarities can be found in the curves plotted in Fig. 2.4. For example, the typical angular width of the spikes is the same for all surfaces. Indeed, in our numerical experiment it is linked to the width L of the illuminated area (which is here equivalent to the coherence domain). The smallest angular period of the fringes formed by the (farthest-off) coherent point-source pair on the surface determines the minimal angular width λ/L of the speckle spikes. This is clearly illustrated in Fig. 2.5, the larger the coherently illuminated area the thinner the angular speckle structures. In optics and radar imaging, sufficiently coherent incident beams (lasers) combined with detectors with fine angular resolution permit to study this phenomenon [14]. In x-ray experiments, the speckle effect can also be visualised in certain configurations. At grazing angles (e.g. $\theta_{\mathrm{sc}} = 1$ mrad), the apparent resolution of the detector $\delta q_x = k_0 \theta \delta\theta$ (see Sect. 4.5.2.1) may be better than $10^{-7} k_0\,\mathrm{m}^{-1}$. The size of the illuminated area being 5 mm, the speckle structures are resolved in the detector.

We now suppose that the illuminated area is increased enough so that the typical angular width of the speckle structures will be much smaller than the angular

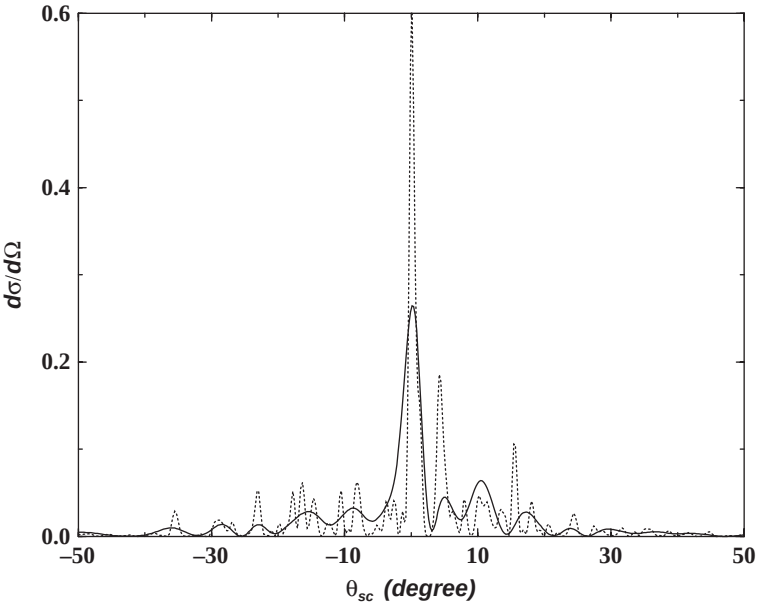

Fig. 2.5 Illustration of the dependence of the angular width of the speckle structures on the size of the illuminated area. Simulation of the intensity angular distribution for one rough surface illuminated in the first case over 60 μm and in the second case over 30 μm. The incident wavelength is 1 μm, the refractive index is $n = 1.5$, normal incidence

resolution of the detector. The detector integrates the intensity over a certain solid angle and, as a result, the fine structures disappear. One notices then that the smooth intensity patterns obtained for all the different surfaces s_n are quite similar. This is not surprising. Indeed, we have seen in the previous paragraph that the finite angular resolution of the detector is equivalent to the introduction of a coherence domain S_{coh} (that is smaller than the illuminated area A). The measured intensity can be considered the incoherent sum of intensities stemming from the different subsurfaces of size S_{coh} that constitute the sample. We now suppose that the illuminated area is big enough to cover many "coherent" subsurfaces, $A > 30S_{\text{coh}}$. Moreover, we suppose that the coherence domain is large enough so that each subsurface presents the same statistical properties $L_{\text{coh}} > 30\xi$, where ξ is the correlation length and L_{coh} the coherence length. If the set of surfaces $\{s_n\}$ can be described by an ergodic stationary process, the ensemble of subsurfaces obtained from one particular realisation s_j will define the same random process with the same ensemble averaging as that created from any other realisation s_k. Consequently, the scattered intensity from one "big" surface s_j can be seen as the ensemble average of the "subsurface" S_{coh} scattered intensity which should be the same for all s_k. This assertion is supported by a comparison between two different numerical treatments of the same scattering experiment [13, 15].

In Fig. 2.6 we have plotted the diffuse intensity obtained from a deterministic rough surface S_j illuminated by a perfectly coherent Gaussian beam, with a detector

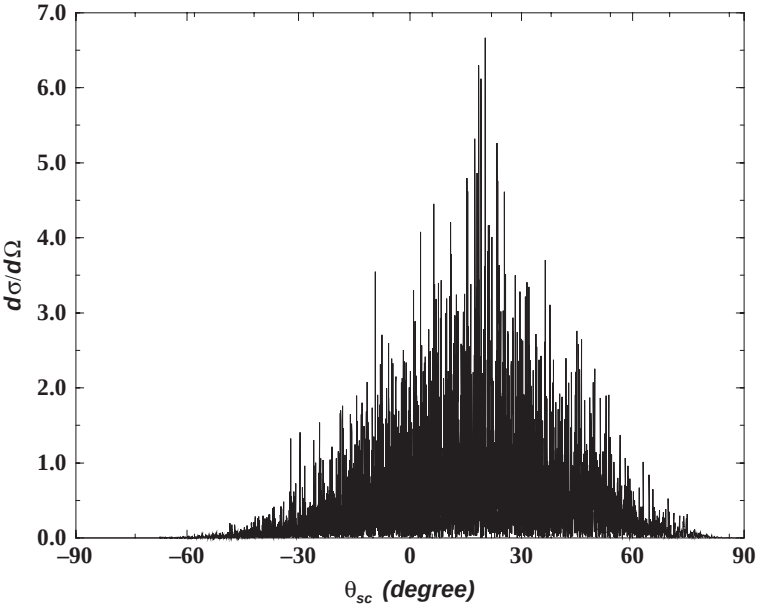

Fig. 2.6 Simulation of the differential scattering cross-section of a rough deterministic surface which is one realisation of a random process. The illuminated area covers 3 mm (roughly several thousands of optical wavelengths). The statistics of the random process are Gaussian height distribution with $\sigma = 0.2\,\mu\text{m}$ and Gaussian correlation function with $\xi = 1\,\mu\text{m}$. The incident wavelength is 1 μm. Courtesy of Prof. M. Saillard [13]

of infinite resolution. The rough surface is one realisation of a random process with Gaussian height distribution function and Gaussian correlation function with correlation length ξ. The incident beam is chosen wide enough so that the illuminated part of S_j is representative of the ergodic random process. In other words, S_j can be divided into many subsurfaces (with similar statistical properties) whose set describes accurately the random process. The total length of the illuminated spot is 5000ξ. It is seen in Fig. 2.6 that the scattered intensity exhibits a very thin speckle pattern. In general these fine structures are not visible. In Fig. 2.7 we have averaged the diffuse intensity over an angular width of 5°, corresponding to the angular resolution of a detector. We compare in Fig. 2.7 the *angular averaged pattern* with the *ensemble average* of the scattered intensity from subsurfaces that are generated with the same random process as S_j but whose coherent illuminated domain is now restricted to 30ξ (i.e. to the coherence domain induced by the finite resolution of the detector). We obtain a perfect agreement between the two scattering patterns. In this example, we no longer need the precise value of the characteristic function $z(\mathbf{r}_\parallel)$ but solely the statistical properties of the random process that describe conveniently these particular surfaces. The integration of the intensity over the solid angle $\Delta\Omega$ will then be replaced by the calculation of the ensemble average of the intensity. This ensemble averaging appears also naturally in the case of surfaces varying with time (such as liquid surfaces like ocean) by recording the intensity during a sufficiently long amount of time.

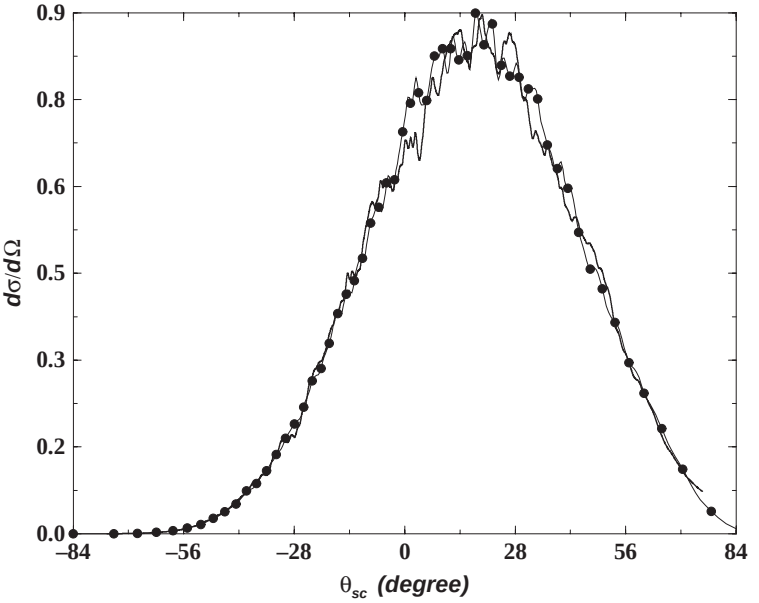

Fig. 2.7 *Solid line*: Angular average over 5° of the differential scattering cross-section of the "big surface" presented in Fig. 2.6; *dotted line*: ensemble average of the differential scattering cross-section of rough surfaces with the same statistics as the "big surface". Size of each realisation is 30 µm, no angular averaging. Courtesy of Prof. Saillard [13]

Each subsurface (either spread spatially via the coherence domains or temporally) generates an electric field **E**. The latter can be viewed as a function of the random process z. The intensity measured by the detector is then related to the mean (in the ensemble averaging sense) square of the field, $\langle|\mathbf{E}|^2\rangle$. The purpose of most wave scattering theories is to evaluate the various moments of **E**. More precisely, the random field can be divided into a mean and a fluctuating part,

$$\mathbf{E} = \langle\mathbf{E}\rangle + \delta\mathbf{E}. \tag{2.45}$$

We usually study separately the different contributions to the intensity.

2.4.2 Notions on Coherent (Specular) and Incoherent (Diffuse) Intensity

In the far field, the scattered electric field $\mathbf{E}_{\mathrm{sc}}$ behaves like a plane wave with wave vector $\mathbf{k}_{\mathrm{sc}}$ and amplitude $\mathbf{E}(\mathbf{k}_{\mathrm{sc}})$, see Eq. (2.32). It can be written as the sum of a mean part and a fluctuating part,

$$\mathbf{E}_{\mathrm{sc}} = \langle\mathbf{E}_{\mathrm{sc}}\rangle + \delta\mathbf{E}_{\mathrm{sc}}. \tag{2.46}$$

The previous discussions have shown that the measured scattered intensity from a rough sample (whose deterministic surface profile is assumed to be one realisation of a given ergodic random process) can be evaluated with the ensemble average of the intensity $\langle|\mathbf{E}_{\rm sc}(\mathbf{k}_{\rm sc})|^2\rangle$,

$$\langle|\mathbf{E}_{\rm sc}|^2\rangle = |\langle\mathbf{E}_{\rm sc}\rangle|^2 + \langle|\delta\mathbf{E}_{\rm sc}|^2\rangle. \tag{2.47}$$

The first term on the right-hand side of Eq. (2.47) is called the coherent intensity while the second term is known as the incoherent intensity. It is sometimes useful to tell the coherent and incoherent processes in the scattered intensity. In the following, we show that the coherent part is a Dirac function that contributes solely to the specular direction [4] if the randomly rough surface is statistically homogeneous in the (Oxy) plane.

In most approximate theories, the random rough surface is of infinite extent and illuminated by a plane wave. Suppose we know the scattered far-field $\mathbf{E}_{\rm sc}$ from a rough surface of defining equation $z = z(\mathbf{r}_\parallel)$. We now address the issue of how $\mathbf{E}_{\rm sc}$ is modified when the whole surface is shifted horizontally by a vector $\mathbf{d}$. It is clear that such a shift will not modify the physical problem. However, the incident wave amplitude acquires an additional phase factor $\exp(i\mathbf{k}_{\rm in}.\mathbf{d})$ and similarly each scattered plane wave $\mathbf{E}_{\rm sc}$ acquires, when returning to the primary coordinates, the phase factor $\exp(-i\mathbf{k}_{\rm sc}.\mathbf{d})$. Thus we obtain,

$$\mathbf{E}_{\rm sc}^{z(\mathbf{r}_\parallel-\mathbf{d})} = e^{-i(\mathbf{k}_{\rm sc}-\mathbf{k}_{\rm in}).\mathbf{d}}\mathbf{E}_{\rm sc}^{z(\mathbf{r}_\parallel)}. \tag{2.48}$$

We now suppose that the irregularities of the rough surface stem from a random spatially homogeneous process. In this case, the ensemble average is invariant under any translation in the (xOy) plane,

$$\left\langle\mathbf{E}_{\rm sc}^{z(\mathbf{r}_\parallel-\mathbf{d})}\right\rangle = \left\langle\mathbf{E}_{\rm sc}^{z(\mathbf{r}_\parallel)}\right\rangle. \tag{2.49}$$

This equality is only possible if

$$\langle\mathbf{E}_{\rm sc}\rangle = A\delta(\mathbf{k}_{\rm sc\parallel} - \mathbf{k}_{\rm in\parallel}). \tag{2.50}$$

Hence, when the illuminated domain (or coherence domain) is infinite, the coherent intensity is a Dirac distribution in the Fresnel reflection (or transmission) direction. For this reason it is also called specular intensity. Note that unlike the coherent term, the incoherent intensity is a function in the $\mathbf{k}_{\rm sc\parallel}$ plane and its contribution in specular direction tends to zero as the detector acceptance is decreased. In real life, the incident beam is space limited, the coherence domain is finite, thus the specular component becomes a function whose angular width is roughly given by $\lambda/L_{\rm coh}$.

In many x-ray experiments, one is solely interested in the specularly reflected intensity. This configuration allows the determination of the z-dependent electron density profile and is often used for studying stratified interfaces (amphiphilic or polymer-adsorbed film). The modelisation of the coherent intensity requires the

evaluation of the single integral Eq. (2.32) that gives the field amplitude while the incoherent intensity requires the evaluation of a double integral Eq. (2.37). It is thus much simpler to calculate only the coherent intensity and many elaborate theories have been devoted to this issue [4]. Chapter 3 of this book gives a thorough description of the main techniques developed for modelling the specular intensity from rough multilayers. However, it is important to bear in mind that the energy measured by the detector about the specular direction comes from both the coherent and incoherent processes inasmuch as the solid angle of collection is non-zero. The incoherent part is not always negligible as compared to the coherent part especially when one moves away from the grazing angles. An estimation of both contributions is then needed to interpret the data.

2.5 Statistical Formulation of the Scattered Intensity Under the Born Approximation

In this last section, we illustrate the notions introduced previously with a simple and widely used model that permits to evaluate the scattering crosssection of random rough surfaces within a probabilistic framework. We discuss the relationship between the scattered intensity and the statistics of the surfaces. The main principles of the Born development have been introduced in Chap. 1, Appendix 1.A, and a complementary approach of the Born approximation is given in Chap. 4 with some insights on the electromagnetic properties of the scattered field.

2.5.1 The Differential Scattering Cross-Section

We start from Eq. (2.32) that gives the scattered far field as the sum of the fields radiated by the induced dipoles in the sample. The main difficulty of this integral is to evaluate the exact field $\mathbf{E}$ inside the scattering object. In the x-ray domain, the permittivity contrast is very small ($\approx 10^{-6}$) and one can assume that the incident field is not drastically perturbed by surrounding radiating dipoles. Hence, a popular assumption (known as the Born approximation) is to approximate $\mathbf{E}$ by $\mathbf{E}_{\text{in}}$. With this approximation the integrand is readily calculated. For an incident plane wave $\mathbf{E}_{\text{in}} e^{-i\mathbf{k}_{\text{in}}.\mathbf{r}}$, the differential scattering cross-section can be expressed as

$$\frac{d\sigma}{d\Omega} = \frac{1}{16\pi^2} \frac{|\mathbf{E}_{\text{in}\perp}|^2}{|\mathbf{E}_{\text{in}}|^2} \int d\mathbf{r} \int d\mathbf{r}' [k^2(\mathbf{r}) - k_0^2][k^2(\mathbf{r}') - k_0^2] e^{i\mathbf{q}.(\mathbf{r}-\mathbf{r}')}, \tag{2.51}$$

where $\mathbf{E}_{\text{in}\perp}$ is the projection of the incident electric field on the plane normal to the direction of observation of the differential cross-section. Denoting the unit vectors in direction $\mathbf{E}_{\text{in}}$ and $\mathbf{E}_{\text{sc}}$, $\widehat{\mathbf{e}}_{\text{in}} = \mathbf{E}_{\text{in}}/E_{in}$ and $(\widehat{\mathbf{e}}_{\text{sc}})^2 = \mathbf{E}_{\text{sc}}/E_{sc}$, respectively, we have $|\mathbf{E}_{\text{in}\perp}| = E_{in}(\widehat{\mathbf{e}}_{\text{in}}.\widehat{\mathbf{e}}_{\text{sc}})^2$. In x-ray experiments, the incident field impinges on the surface at grazing angle and one studies the scattered intensity in the vicinity

of the specular component. In this configuration, the orthogonal component of the incident field with respect to the scattered direction is close to the total incident amplitude. Yet, we retain the projection term $(\widehat{\mathbf{e}}_{\rm in}.\widehat{\mathbf{e}}_{\rm sc})^2$ in the differential scattering cross-section for completeness and coherence with the results of Chap. 1. Bearing in mind the value of the permittivity contrast as a function of the electronic density, Eq. (2.31), Eq. (2.51) simplifies to

$$\frac{d\sigma}{d\Omega} = r_e^2(\widehat{\mathbf{e}}_{\rm in}\,\widehat{\mathbf{e}}_{\rm sc})^2 \int d\mathbf{r} \int d\mathbf{r}' \rho_{el}(\mathbf{r})\rho_{el}(\mathbf{r}')e^{i\mathbf{q}.(\mathbf{r}-\mathbf{r}')}, \tag{2.52}$$

with ρ_{el} the electron density and r_e the classical electron radius.[4] In the case of a rough interface separating two semi-infinite homogeneous media one gets,

$$\frac{d\sigma}{d\Omega} = r_e^2\rho_{el}^2(\widehat{\mathbf{e}}_{\rm in}.\widehat{\mathbf{e}}_{\rm sc})^2 \int_{-\infty}^{z(\mathbf{r}_\parallel)} dz \int_{-\infty}^{z(\mathbf{r}'_\parallel)} dz' \int d\mathbf{r}_\parallel \int d\mathbf{r}'_\parallel e^{i\mathbf{q}.(\mathbf{r}-\mathbf{r}')}. \tag{2.53}$$

Integrating Eq. (2.53) over (z,z') (with the inclusion of a small absorption term to ensure the convergence at $-\infty$) yields,

$$\frac{d\sigma}{d\Omega} = \frac{\rho_{el}^2 r_e^2}{q_z^2}(\widehat{\mathbf{e}}_{\rm in}.\widehat{\mathbf{e}}_{\rm sc})^2 \int d\mathbf{r}_\parallel \int d\mathbf{r}'_\parallel e^{i\mathbf{q}_\parallel.(\mathbf{r}_\parallel-\mathbf{r}'_\parallel)} e^{iq_z\left[z(\mathbf{r}_\parallel)-z(\mathbf{r}'_\parallel)\right]}. \tag{2.54}$$

This equation concerns a priori the scattering from any (deterministic or not) object. In this chapter, we are mostly interested by the scattering from surfaces whose surface profile z is unknown or of no interest. We have seen in the preceding sections that if z is described by a random homogeneous ergodic process, the intensity measured by the detector can be approximated by the ensemble average of the scattering cross-section. It amounts to replacing in Eq. (2.54) the integration over the surface by an ensemble average, $\int f(\mathbf{r}_\parallel)d\mathbf{r}_\parallel = L_xL_y\langle f\rangle$, where L_x, L_y are the dimensions of the surface along *Ox* and *Oy*. One obtains,

$$\frac{d\sigma}{d\Omega} = \frac{\rho_{el}^2 r_e^2 L_xL_y}{q_z^2}(\widehat{\mathbf{e}}_{\rm in}.\widehat{\mathbf{e}}_{\rm sc})^2 \int d\mathbf{r}_\parallel e^{i\mathbf{q}_\parallel.\mathbf{r}_\parallel} \left\langle e^{iq_z\left[z(\mathbf{r}_\parallel)-z(\mathbf{0}_\parallel)\right]}\right\rangle. \tag{2.55}$$

[4] One can make a general presentation of elastic scattering under the Born approximation from the scattering by an isolated object as presented in Sect. 1.2.4 and Appendix 1.A. The differential scattering cross-section can be cast in the form

$$\frac{d\sigma}{d\Omega} = \left|\sum_j be^{i\mathbf{q}.\mathbf{r}_j}\right|^2 = \left|\int d\mathbf{r}\rho be^{i\mathbf{q}.\mathbf{r}}\right|^2,$$

where ρ is the density of scattering objects and b their scattered length as introduced in Eq. (1.34). The complex exponential is the result of the phase shift between waves scattered in the $\mathbf{k}_{\rm sc}$ direction by scatterers separated by a vector $\mathbf{r}$ as shown in Fig. 2.8. For neutrons, b is the scattering length which takes into account the strong interaction between the neutrons and the nuclei (we do not consider here magnetic materials); for x-rays, $b = r_e = (e^2/4\pi\epsilon_0 m_e c^2) = 2.8\times10^{-15}$ m which is the classical radius of the electron.

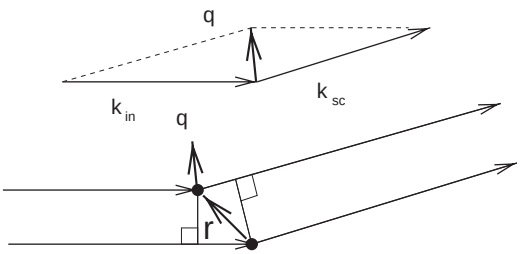

Fig. 2.8 Phase shift between the waves scattered by two point scatterers separated by a vector $\mathbf{r}$. The phase shift is $(\mathbf{k}_{sc}-\mathbf{k}_{in}).\mathbf{r}=\mathbf{q}.\mathbf{r}$

Note that the expression (2.55) of the differential scattering cross-section accounts for both the coherent and incoherent processes. Hence, this integral does not converge in the function sense, it contains a Dirac distribution if the surface is infinite. This property will be illustrated with various examples in the following. If the probability density of z is Gaussian, we can write the differential cross-section as

$$\frac{d\sigma}{d\Omega}=\frac{\rho_{el}^2 r_e^2 L_x L_y}{q_z^2}(\widehat{\mathbf{e}}_{in}.\widehat{\mathbf{e}}_{sc})^2\int d\mathbf{r}_{\parallel}e^{i\mathbf{q}_{\parallel}.\mathbf{r}_{\parallel}}e^{-\frac{1}{2}q_z^2\left\langle\left[z(\mathbf{r}_{\parallel})-z(\mathbf{0}_{\parallel})\right]^2\right\rangle}. \tag{2.56}$$

We see that, under the Born approximation (where we neglect multiple scattering) the scattered intensity is related to the Fourier transform of the exponential of the pair-correlation function, $g(r_{\parallel})=\left\langle\left[z(\mathbf{r}_{\parallel})-z(\mathbf{0}_{\parallel})\right]^2\right\rangle$. In the following we illustrate this result by studying the differential scattering crosssection for various pair-correlation functions. We start by the expression of the scattering differential cross-section in the case of a flat surface.

2.5.2 Ideally Flat Surfaces

For ideally flat surfaces $g(r_{\parallel})$ is zero everywhere at the surface and the scattering cross-section yields

$$\frac{d\sigma}{d\Omega}=\frac{r_e^2\rho_{el}^2 L_x L_y}{q_z^2}(\widehat{\mathbf{e}}_{in}.\widehat{\mathbf{e}}_{sc})^2\int d\mathbf{r}_{\parallel}e^{i\mathbf{q}_{\parallel}.\mathbf{r}_{\parallel}}. \tag{2.57}$$

The integral is the Fourier transform of a constant so that,[5]

$$\frac{d\sigma}{d\Omega}=\frac{4\pi^2 r_e^2\rho_{el}^2 L_x L_y}{q_z^2}(\widehat{\mathbf{e}}_{in}.\widehat{\mathbf{e}}_{sc})^2\delta(\mathbf{q}_{\parallel}). \tag{2.58}$$

The scattered intensity is thus a Dirac distribution in the Fresnel reflection direction. As expected, for a perfectly flat surface, the reflectivity comes solely from a

[5] Let us recall that $\delta(\mathbf{q}_{\parallel})=\frac{1}{4\pi^2}\int e^{-i\mathbf{q}_{\parallel}.\mathbf{r}_{\parallel}}d\mathbf{r}_{\parallel}$.

coherent process (Sect. 2.4.2), the incoherent scattering is null $\langle \delta E^2 \rangle = 0$. Note that the reflectivity decreases as a power law with q_z. We now turn to the more complicated problem of scattering from rough surfaces that are described statistically by a homogeneous ergodic random process.

2.5.3 Self-Affine Rough Surfaces

2.5.3.1 Surfaces Without Cut-Off

We first consider self-affine rough surfaces with pair-correlation function g given by Eq. (2.24), $g(r_\parallel) = A_0 r_\parallel^{2h}$. With this pair-correlation function, the roughness cannot be determined since there is no saturation. The scattering cross-section is in this case,

$$\frac{d\sigma}{d\Omega} = \frac{r_e^2 \rho_{el}^2 L_x L_y}{q_z^2} (\hat{\mathbf{e}}_{\text{in}}.\hat{\mathbf{e}}_{\text{sc}})^2 \int d\mathbf{r}_\parallel e^{-\frac{q_z^2}{2} A R^{2h}} e^{i\mathbf{q}_\parallel \cdot \mathbf{r}_\parallel}, \tag{2.59}$$

and can be expressed in polar coordinates as

$$\frac{d\sigma}{d\Omega} = \frac{r_0^2 \rho_e^2 L_x L_y}{q_z^2} (\hat{\mathbf{e}}_{\text{in}}.\hat{\mathbf{e}}_{\text{sc}})^2 \int dr_\parallel e^{-\frac{q_z^2}{2} A R^{2h}} J_0(q_\parallel r_\parallel), \tag{2.60}$$

with $q_\parallel$ being the modulus of the in-plane scattering wave vector and J_0 the zeroth order Bessel function. The above integral has analytical solutions for $h = 0.5$ and $h = 1$ and has to be calculated numerically in other cases. For $h = 1$, the integration yields,

$$\frac{d\sigma}{d\Omega} = \frac{r_e^2 \rho_{el}^2 L_x L_y}{q_z^2} (\hat{\mathbf{e}}_{\text{in}}.\hat{\mathbf{e}}_{\text{sc}})^2 e^{-q_\parallel^2/q_z^4}, \tag{2.61}$$

and for $h = 0.5$,

$$\frac{d\sigma}{d\Omega} = (\hat{\mathbf{e}}_{\text{in}}.\hat{\mathbf{e}}_{\text{sc}})^2 \frac{r_e^2 \rho_{el}^2 L_x L_y}{q_z^2} \frac{\pi A}{\left(q_\parallel^2 + \left(\frac{A}{2}\right)^2 q_z^4\right)^{3/2}}. \tag{2.62}$$

The above expressions clearly show that for surfaces of this kind the scattering is purely diffuse (no Dirac distribution, no specular component).

2.5.3.2 Surfaces with Cut-Off

Rough surfaces are said to present a cut-off length when the correlation function $C_{zz}(\mathbf{r}_\parallel)$ tends to zero when $r_\parallel$ increases (for example see Eq. (2.26), when $C_{zz}(r_\parallel) = \sigma^2 \exp\left(-\frac{r_\parallel^{2h}}{\xi^{2h}}\right)$, the cut-off is ξ). In this general case an analytical calculation is not possible and the scattering cross-section becomes,

$$\frac{d\sigma}{d\Omega} = \frac{r_e^2 \rho_{el}^2 L_x L_y}{q_z^2} e^{-q_z^2\sigma^2} (\widehat{\mathbf{e}}_{\text{in}}.\widehat{\mathbf{e}}_{\text{sc}})^2 \int d\mathbf{r}_{\parallel} e^{q_z^2 C_{zz}(\mathbf{r}_{\parallel})} e^{i\mathbf{q}_{\parallel}.\mathbf{r}_{\parallel}}. \tag{2.63}$$

The integrand in Eq. (2.63) does not tend to 0 when $\mathbf{r}_{\parallel}$ is increased. The integration over an infinite surface does not exist in the function sense. Indeed, $d\sigma/d\Omega$ accounts for both the coherent and incoherent contributions to the scattered power. It is possible to extract the specular (coherent) and the diffuse (incoherent) components by writing the integrand in the form,

$$e^{q_z^2 C_{zz}(\mathbf{r}_{\parallel})} = 1 + \left(e^{q_z^2 C_{zz}(\mathbf{r}_{\parallel})} - 1 \right). \tag{2.64}$$

The distributive part (or Dirac function) characterises the coherent or specular reflectivity while the regular part gives the diffuse power. Equation (2.63) is then cast in the form,

$$\frac{d\sigma}{d\Omega} = \left(\frac{d\sigma}{d\Omega} \right)_{\text{coh}} + \left(\frac{d\sigma}{d\Omega} \right)_{\text{incoh}}, \tag{2.65}$$

with

$$\begin{aligned} \left(\frac{d\sigma}{d\Omega} \right)_{\text{coh}} &= \frac{r_e^2 \rho_{el}^2 L_x L_y}{q_z^2} e^{-q_z^2\sigma^2} (\widehat{\mathbf{e}}_{\text{in}}.\widehat{\mathbf{e}}_{\text{sc}})^2 \int d\mathbf{r}_{\parallel} e^{i\mathbf{q}_{\parallel}.\mathbf{r}_{\parallel}} \\ &= \frac{4\pi^2 r_e^2 \rho_{el}^2 L_x L_y}{q_z^2} e^{-q_z^2\sigma^2} \delta(\mathbf{q}_{\parallel}) (\widehat{\mathbf{e}}_{\text{in}}.\widehat{\mathbf{e}}_{\text{sc}})^2 \end{aligned} \tag{2.66}$$

and

$$\left(\frac{d\sigma}{d\Omega} \right)_{\text{incoh}} = \frac{r_e^2 \rho_{el}^2 L_x L_y}{q_z^2} e^{-q_z^2\sigma^2} (\widehat{\mathbf{e}}_{\text{in}}.\widehat{\mathbf{e}}_{\text{sc}})^2 \int d\mathbf{r}_{\parallel} \left(e^{q_z^2 C_{zz}(\mathbf{r}_{\parallel})} - 1 \right) e^{i\mathbf{q}_{\parallel}.\mathbf{r}_{\parallel}}. \tag{2.67}$$

The specular part is similar to that of a flat surface except that it is reduced by the roughness Debye–Waller factor $e^{-q_z^2\sigma^2}$. The diffuse scattering part may be determined numerically if one knows the functional form of the correlation function. When $q_z^2 C_{zz}(\mathbf{r}_{\parallel})$ is small, the exponential can be developed as $1 + q_z^2 C_{zz}(\mathbf{r}_{\parallel})$. In this case, the differential scattering cross-section appears to be proportional to the power spectrum of the surface $P(\mathbf{q}_{\parallel})$,

$$\left(\frac{d\sigma}{d\Omega} \right)_{\text{incoh}} = r_e^2 \rho_{el}^2 L_x L_y e^{-q_z^2\sigma^2} 4\pi^2 P(\mathbf{q}_{\parallel}) (\widehat{\mathbf{e}}_{\text{in}}.\widehat{\mathbf{e}}_{\text{sc}})^2. \tag{2.68}$$

We see with Eqs. (2.66) and (2.68) that the Born assumption permits to evaluate both the coherent and incoherent scattering cross-sections of rough surfaces in a relatively simple way. This technique can be applied without additional difficulties to more complicated structures such as multilayers or inhomogeneous films. Unfortunately, in many configurations, the Born assumption proves to be too restrictive and one can miss major features of the scattering process. More accurate models

such as the distorted-wave Born approximation have been developed and are presented in Chap. 4 of this book. Yet, the expressions of the coherent and incoherent scattering cross-sections given here by the first Born approximation provide useful insights on how the measured intensity relates to the shape (statistics) of the sample. The coherent reflectivity, Eq. (2.66), does not give direct information on the surface lateral fluctuations, except for the overall roughness σ, but it provides the electronic density of the plane substrate. Hence, reflectivity experiments are used in general to probe, along the vertical axis, the electronic density of samples that is roughly homogeneous in the (xOy) plane but varies in a deterministic way along Oz (e.g. typically multilayers). Chapter 3 of this book is devoted to this issue. On the other hand the incoherent scattering Eq. (2.68) is directly linked to the height–height correlation function of the surface. Bearing in mind the physical meaning of the power spectrum, Sect. 2.2.3, we see that measuring the diffuse intensity at increasing $q_{\|}$ permits to probe the surface state at decreasing lateral scales. Hence, scattering experiments can be a powerful tool to characterise the rough sample in the lateral (Oxy) plane. This property will be developed and detailed in Chap. 4.

References

1. Beckmann, P., Spizzichino, A.: The Scattering of Electromagnetic Waves from Rough Surfaces. Pergamon Press, Oxford, UK (1963).
2. Bass, F.G., Fuks, I.M.: Wave Scattering from Statistically Rough Surfaces. Pergamon, New York (1979).
3. Ogilvy, J.A.: Theory of Wave Scattering from Random Rough Surfaces. Adam Hilger, Bristol, UK (1991).
4. Voronovich, G.: Wave Scattering from Rough Surfaces. Springer-Verlag, Berlin (1994).
5. Mandel, L., Wolf, E.: Optical Coherence and Quantum Optics. Cambridge University Press, Cambridge, USA (1995).
6. Guérin, C.A., Holschneider, M., Saillard, M.: Waves Random Media, **7**, 331–349 (1997).
7. Mandelbrodt, B.B.: The Fractal Geometry of Nature. Freeman, New York (1982).
8. Born, M., Wolf, E.: Principle of Optics. Pergamon Press, New York (1980).
9. Oxtoby, D.W., Novack, F., Rice, S.A.: J. Chem. Phys. **76**, 5278 (1982).
10. Sinha, S.K., Tolan, M., Gibaud, A.: Phys. Rev. B **57**, 2740 (1998)
11. Nieto-Vesperinas, M., Dainty, J.C.: Scattering in Volume and Surfaces. Elsevier Science Publishers, B. V. North-Holland (1990).
12. Petit, R. (ed.): Electromagnetic Theory of Gratings. Topics in Current Physics. Springer Verlag, Berlin (1980).
13. Saillard, M., Maystre, D.: J. Opt. Soc. Am. A, **7**(6), 982–990 (1990).
14. Dainty, J.C. (ed.): Laser speckle and Related Phenomena. Topics in Applied Physics. Springer-Verlag, New York (1975).
15. Saillard, M., Maystre, D.: J. Opt. **19**, 173–176, (1988).